Robust Imaging-Free Object Recognition Through Anderson Localizing Optical Fiber

Xiaowen Hu, Jian Zhao, Jose E. Antonio-Lopez, Shengli Fan, Rodrigo Amezcua Correa, and Axel Schülzgen, *Fellow, IEEE*

(Invited Paper)

***Abstract*—Recognizing objects directly from optical fiber output images is useful in endoscopic applications when forming a clear image of the object is unnecessary or rather difficult. Conventional fiber-optic systems, such as multicore-fiber-based and multimode-fiber-based systems, suffer from the sensitivity of the fiber to external perturbations. For example, a slight movement of the fiber (a-few-millimeters translation of the tip for meter-long multicore fibers or multimode fibers) can greatly change the output images of the system. In this work, we utilize the light guidance stability of recently proposed glass-air Anderson localizing optical fiber (GALOF) to achieve robust imaging-free objection recognition. We transport five classes of cell images through an 80-cm straight GALOF. A deep convolutional neural network is trained to classify the output images and tested on images never seen, namely, images collected when the fiber is bent or when the fiber facet is placed several millimeters away from the object without any distal optics. Bending-invariant high classification accuracy (86.8% on average) is observed all the way to the maximum bending offset distance of 45 cm (∼74thinsp;° bending angle). High classification accuracy (91.2%) is also preserved when the fiber facet is 0.5 mm away from the object.**

***Index Terms*—Microstructured optical fiber, deep learning, object recognition, transverse Anderson localization.**

I. Introduction

FIBER-OPTIC imaging systems (FOISs) are the backbone of modern endoscopy for bio-imaging research as well as medical diagnosis [1], [2] due to their miniature sizes and flexibility. The imaging unit of FOISs can penetrate deeply into tissues and organs with minimal invasions to study areas inaccessible by conventional microscopy. Moreover, FOISs can be implanted in freely moving animals [3], thus, enabling real-time *in vivo* imaging. The two most commonly used optical fibers in FOISs are multicore fibers (MCFs) [4]–[12] and multimode fibers (MMFs) [13]–[16]. A typical MCF contains thousands of closely spaced cores in a common cladding, whereas an MMF contains a single step-index or graded-index core that supports thousands of modes. With the recent development of machine learning, researchers and doctors begin to benefit from computer-aided diagnosis (CAD) in FOIS-based imaging. Conventional CAD in FOISs consists of two phases: image acquisition and image classification [8], [17]. In the image acquisition phase, a high-quality image of the object is formed. This is straightforward in MCF-based FOISs since images are sampled and transmitted directly through individual fiber cores. For MMF-based FOISs, however, images are encoded into thousands of optical modes that travel at different speeds along the fiber. The output speckle patterns of the MMF contain the information about the object image. Several solutions have been proposed to recover the input images. A complex-valued transmission matrix (TM) [13], [14], [16], [18]–[21] can be obtained experimentally to establish the relationship between the input orthogonal bases and the output bases. The speckle patterns are then inverted back to recover the original images. Deep convolutional neural networks (DCNNs) can be trained to directly "learn" the mapping between the input images and speckle patterns, and then reconstruct input images from speckle patterns [22]–[24]. A third method is a combination of the last two. It approximates the TM from the input image and speckle pattern pairs using a learning-based algorithm [25]. In the image classification phase, traditional machine learning classifiers learn to recognize patterns in image features handcrafted by human experts. Nowadays, deep learning [26] can differentiate high-level features through self-directed learning and outperforms conventional methods. Therefore, deep learning has become the state of the art and has been widely implemented in biomedical image classifications [27]–[29].

Despite the great success of conventional CAD in FOISs, it has a few drawbacks. For deep-learning-based image reconstruction, a large number of input-output image pairs needs to be collected during the image acquisition phase. This requires a reference arm in the setup, which makes the calibration complicated and demanding. Under some circumstances, it is even impossible to get access to the ground truth images. Yet, since the speckle patterns contain as much information as the original images, there is no fundamental reason to reconstruct

Manuscript received July 15, 2020; revised October 5, 2020; accepted October 5, 2020. Date of publication July 10, 2020; date of current version February 16, 2021. The authors received no specific funding for this work. *(Corresponding author: Jian Zhao.)*

Xiaowen Hu, Jose E. Antonio-Lopez, Shengli Fan, Rodrigo Amezcua Correa, and Axel Schülzgen are with the University of Central Florida, Orlando, FL 32816 USA (e-mail: steven.hu@knights.ucf.edu; jealopez@creol.ucf.edu; shengli.fan@knights.ucf.edu; r.amezcua@creol.ucf.edu; axel@creol.ucf.edu).

Jian Zhao is with the University of Central Florida, Orlando, FL 32816 USA and also with Boston University, Boston, MA 02215 USA (e-mail: jianzhao@knights.ucf.edu).

Color versions of one or more of the figures in this article are available online at https://ieeexplore.ieee.org.

Digital Object Identifier 10.1109/JLT.2020.3029416

the original images before classification. Objects can be directly recognized from the speckle patterns [30]–[34]. The concept of imaging-free object recognition through optical fibers can be traced back to the early 90's [35]–[37], when artificial neural networks were applied to classify speckle patterns from MMFs. With the aid of deep learning, researchers are now able to classify speckle patterns resulting from more complicated input images in MMFs [23], [38]–[40] and MCFs [41]. One may argue that deep-learning-enabled image reconstruction is not necessary when MCFs are used or when the TM method is adopted to recover images in MMFs. However, conventional FOISs face another major challenge. Strong core-to-core mode coupling in MCFs [9]–[12], [42], [43] and multimode interferences in MMFs make them very susceptible to external perturbations, such as fiber movement (translation of a few millimeters in the fiber tip for meter-long MCFs or MMFs [10], [14], [16], [44]) or thermal variations (about 15 °C for MMF [16]), which greatly change the output images of the systems. Efforts have been made in both TM [21], [45]–[50], and deep learning methods [23], [51] to alleviate this adverse effect. Nevertheless, the sensitivity to external perturbations is intrinsic in the fiber properties and is rather hard to get rid of.

Recently emerging Anderson localizing optical fibers [52]–[61] pave the way to realize robust imaging-free object recognition through FOISs. The refractive index distribution in Anderson localizing optical fibers is disordered in the transverse plane and homogenous along the light propagation direction. Because of transverse Anderson localization (TAL), Anderson localizing optical fibers can support thousands of modes embedded in the random structure through multiple scattering process. Unlike the modes in conventional MMFs or MCFs, the TAL-supported modes demonstrate single-mode-like properties, such as bending-invariance and high spatial coherence [59], [60], [62]. Each of these modes also corresponds to a beam propagation channel, which constitutes the foundation of high-quality robust imaging system [63], [64]. The mode density in TAL fiber ($\sim$10 modes/μm^2) is orders of magnitude higher than that in MCFs ($\sim$0.1 modes/μm^2) or MMFs ($\sim$1 mode/μm^2) [62], thus, enabling transport of more complex images, e.g. cell images [60]. Moreover, the effective beam width in the transverse plane, also known as localization length, has been shown to be independent of wavelength [65]. It makes incoherent broadband illumination possible, which is extremely challenging in systems based on MCFs or MMFs. In our previous work [59], [60], we have demonstrated the robust and high-fidelity imaging capabilities of glass-air Anderson localizing optical fibers (GALOFs) to transport cell images under mechanical bending, temperature fluctuations, or variations on the imaging depth between the fiber facet and the object. In this work, we further exploit the unique GALOF properties to achieve robust imaging-free object recognition. Object recognition is often considered a task that is more perturbation tolerant than image reconstruction since it only involves extracting and differentiating features from various objects, whereas image reconstruction requires pixel-wise accuracy. Objects can still be recognized even though their images are blurry. Thus, more robustness is expected in an object recognition task, as is confirmed in this work. We transport five classes of cell images through an 80-cm straight GALOF with the distal fiber end touching the object and train a DCNN to classify the output images. Then we test the DCNN classifier with output images collected when the fiber is strongly bent or when the fiber facet is moved a few millimeters away from the object. High classification accuracy is preserved in both cases, on average 86.8% with the maximum bending angle of $\sim$74 ° and 91.2% for a detecting depth of 0.5 mm.

II. Methods

A. Experiments

The scanning electron microscope (SEM) image of the GALOF used in the experiments is shown in Fig. 1(e). It is fabricated using the stack-and-draw method. The disordered structure is about 278 μm in diameter, with an air-hole-filling fraction of $\sim$28.5% [58]. The length L of the fiber is 80 cm. Fig. 1(a)–(c)show the experimental setup and workflows under different conditions when the fiber is straight, away from the object, and bent, respectively. In all cases, we illuminate five different classes of samples with an LED centered at 460 nm. Fig. 1(d) I-V show bright-field microscopy images of these samples, i.e., I: bird blood cell, II: frog blood cell, III: polymer microsphere, IV: human red blood cell, V: cancerous human stomach cell. The region of interest (ROI) in the sample is first magnified by a 10x microscope objective MO1 (NA = 0.3) and a tube lens L1 (f = 200 mm) before being transported through the GALOF. The image of the fiber output facet is projected onto a CCD camera (Manta G-145B, 30 fps) by a 20x microscope objective MO2 (NA = 0.75) and a tube lens L2 (f = 200 mm). The collected 8-bit grayscale image is then cropped to a size of 420 × 420 pixels. As an example, Fig. 1(f) show the output images from the five types of sample images when the GALOF is kept straight. Each output image is labeled with the corresponding sample class as the ground truth. The cell samples are scanned both horizontally and vertically with 5 μm step to generate various images. In depth object recognition (Fig. 1(b)), the fiber input end is placed away from the object with a depth ranging from 0.5 mm to 4 mm with a step of 0.5 mm. In the fiber-bent experiment (Fig. 1(c)), the amount of bending is quantified by the offset distance d. The corresponding bending angle θ can be calculated from $1 - d\theta/L = \cos\theta$. Starting from 5 cm, the offset distance is increased in a 5 cm step all the way to 45 cm, which corresponds to the largest bending angle of $\sim$74 °. We collect 45,000 images, 9,000 for each class, from the straight fiber to establish the training dataset. The validation set consists of 2,000 different images, 400 for each class, collected from the straight fiber. Lastly, for each detecting depth and bending offset distance, as well as the straight fiber, we collect separate 2,000 images, 400 for each class, to form the test sets.

B. Data Preprocessing

As can been seen in Fig. 1(f), similar patterns appear in all collected output images. However, mechanical shifts and vibrations of the setup during the experiments lead to tiny displacements among these images. To ensure consistency, all images in the training set, validation set, and test sets are registered according to an arbitrarily chosen image in the training set using the

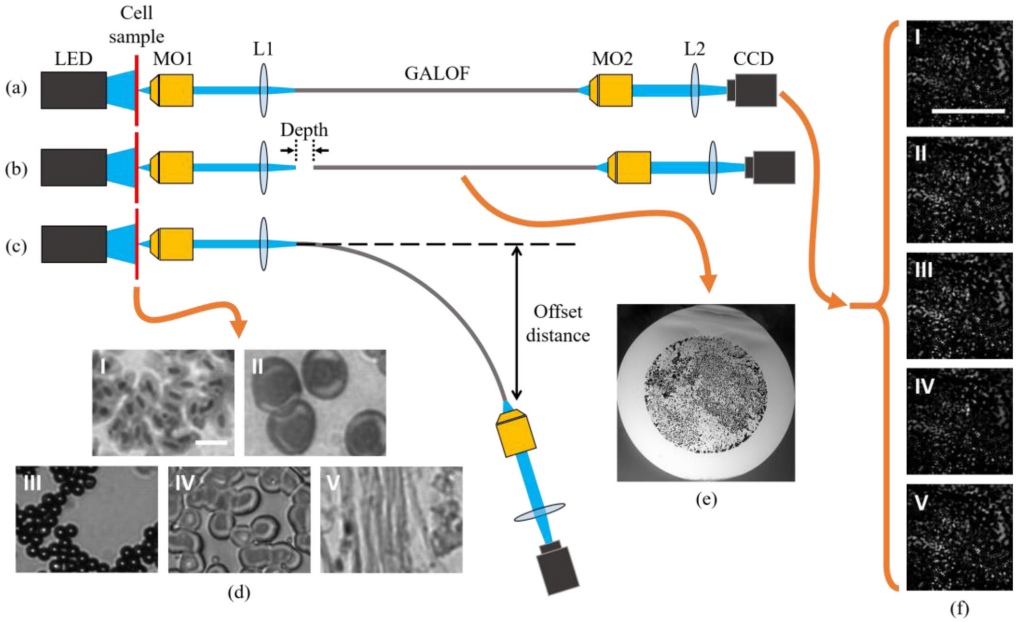

Fig. 1. (a–c): Schematic diagram of the experimental setup under the condition of (a) the GALOF is kept straight; (b) the input facet of the GALOF is located at various depths away from the back focal plane of Lens L1; (c) the GALOF is bent with different offset distances while the input facet is fixed. MO: microscope objective; L: tube lens. (d): Sampled images from the five classes of samples used in the experiments: (I) bird blood cell, (II) frog blood cell, (III) polymer microsphere, (IV) human red blood cell, and (V) cancerous human stomach cell. (e): SEM image of the GALOF. (f): Examples of output images from the straight GALOF when class I to class V samples are transported, respectively. The scale bars in d(I) and f(I) are both 10 μm long.

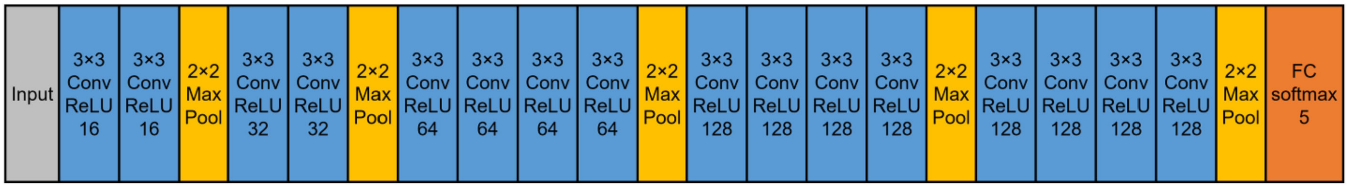

Fig. 2. The architecture of the DCNN classifier. Gray block: the network input of size 224 × 224 × 1. Blue block: convolutional layers. For example, the first blue block means it consists of 16 3 × 3 convolutional filters with rectified linear unit (ReLU) as the activation function. Yellow block: 2 × 2 max-pooling layer with a stride of 2. Orange block: fully connected layer containing five output units with softmax activation function.

Matlab *imregister* function. Monomodal image registration and translation geometric transformation are applied. The registered images are then resized to 224 × 224 with the anti-aliasing. Our results show that resizing the images does not degrade the classification performance. Finally, standardization is applied to all the images by subtracting the training set mean and dividing by the training set standard deviation. The corresponding ground truth labels of the images are converted to vectors using one-hot encoding. Each vector contains five elements: '1' for the true class and '0' for the others.

C. DCNN Implementation

To classify the preprocessed images, we build a VGG19-type [66] DCNN. The DCNN has an architecture with alternating convolutional and max-pooling layers (Fig. 2). The convolutional layers consist of small 3 × 3 convolutional filters. The number of filters in the layers increases as the network goes deeper. The output of the convolutional downsampling encoder is passed through a fully connected layer with softmax activation function. The fully connected layer has five output units, which can be explained as the predicted possibilities of an input image belonging to certain classes. We train the DCNN with the 45,000 image-label pairs. The weights in the DCNN are initialized using the Glorot normal initializer [67]. An adaptive moment estimation (Adam) [68] optimizer with a learning rate of 1×10^{-5} is used to minimize the categorical cross entropy loss function. During the training, dropout [69] with a rate of 0.4 is implemented after each convolutional layer and before the fully-connected layer to prevent overfitting. The DCNN is trained for 200 epochs. In each epoch, the training pairs are shuffled and split into batches of size 128. The DCNN is trained in parallel with two GPUs (GeForce GTX 1080 Ti). After training, all the weights in the DCNN are fixed. During test, given a new input image that has never been "seen" before, the DCNN chooses the class with the maximum possibility as its prediction.

Despite the robustness of GALOF, there is still some inconsistency among the training set and test sets, which is due to tiny movements of the optical components during the experiments and, in depth object recognition, diffraction of the images over some distance. Therefore, great care must be taken to prevent the DCNN classifier from overfitting the training set. First,

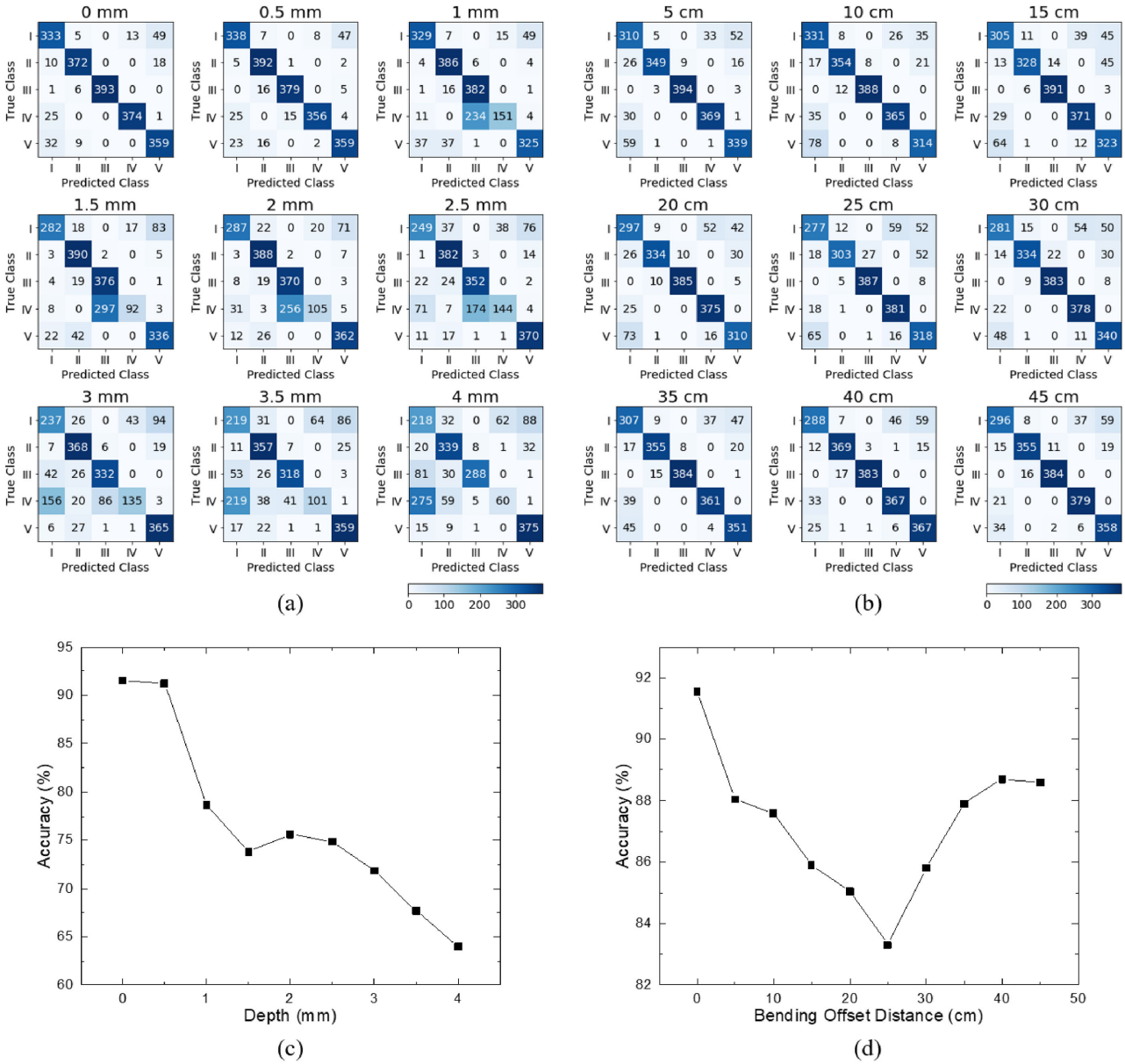

Fig. 3. (a), (b): Confusion matrices of the predicted classes and true classes for various detecting depths and bending offset distances, respectively. (c), (d): The classification accuracy as a function of detecting depth and bending offset distance, respectively. In both plots, the classification accuracy starts at 91.55%, which is the classification accuracy for the test images collected with a straight fiber and the object located directly at the input fiber facet.

among all the DCNNs that achieve similar performances on the training set, we choose the one with the minimal number of weights. Specifically, we reduce the number of filters used in the convolutional layers until the final classification accuracy drops on the training set. Secondly, early stopping is used. That is, we stop training the DCNN when convergence is observed. These two methods are known to be effective in generalizing DCNNs.

III. Results and Discussions

We evaluate the DCNN classifier on the test sets. Fig. 3(a), (b) show the confusion matrices of the predicted classes and true classes for various detecting depths and bending offset distances. The corresponding changes of accuracy, defined as the percentage of correctly recognized objects, are shown in Fig. 3(c), (d). It can be seen that high classification accuracy (91.2%) is preserved at a detecting depth of 0.5 mm. The classification accuracy drops as the detecting depth gets larger, which might be attributed to the loss of high-frequency information of the object under incoherent illumination. In particular, an increasing misclassification of class IV object as class III and class I objects is found. Nevertheless, high classification accuracy (>85%) is retained for class II and V objects even for large detecting depths between the object and the input fiber facet.

On the other hand, no obvious degradation in classification performance is observed when the bending offset distance is increased. High classification accuracy with an average of 86.8%

is maintained from the offset distance of 5 cm to the maximum offset distance of 45 cm. The valley point at 25 cm is most likely due to experimental errors, for instance, slight movements of optical exponents. Most notable confusions are between class I, class IV and V objects.

The consistent bending-invariant classification performance of the GALOF-based FOIS demonstrates its suitability for many practical endoscopy applications that require a high degree of flexibility. The robustness of our system on object classification can be directly related to the single-mode properties of the densely packed transversely localized modes in the GALOF [62], [64]. It has been shown that these localized modes can potentially resist extremely small bending radii ($\sim$1 mm) [70], resulting in consistent fiber output images. In contrast, a slight fiber movement (several millimeters in the fiber tip translation for meter-long MCFs or MMFs [10], [14], [16], [44]) can change the output images of MCF-based or MMF-based FOISs, and consequently, affect their performances on image acquisition tasks. As a result, the length of optical fibers used in current in vivo imaging applications is limited to several centimeters [20]. Efforts have been made to increase robustness in MMF-based FOISs by including perturbations, such as mechanical bending, temperature fluctuations and wavelength drifts, into the training set when the DCNN is trained [23], [40], [51]. However, this does not generalize the systems to situations that have not been encountered during the training. Small deviations from the conditions included in the training set will still degrade the performance due to the very strong dependence of the multimode interference in MMFs on external environment. Contrarily, using our GALOF-based FOIS, the DCNN classifier is trained exclusively with the data collected from the straight fiber and performs astonishingly well on unseen data. Again, this robustness in performance is a direct result of the unique intrinsic GALOF properties. Besides, the GALOF-based system is also expected to maintain high classification accuracy under temperature variations. As shown in our previous work [60], the quality of reconstructed images is not affected by thermal changes over a range of 30 °C, whereas temperature shifts of 15 °C can greatly impair the performance of MMF-based systems [16]. Moreover, the ability of GALOF-based systems to accurately recognize and classify objects that are located several millimeters away from the fiber facet without the need for any distal optics can eliminate contact damage as well as minimize collateral penetration damage, since the size of the fiber probe unit can be as small as the outer fiber diameter.

Although the effect of fiber bending is investigated in our previous paper [60] and in this work, these two studies are related to different imaging problems: image reconstruction versus image classification. The design of the deep learning algorithm for image classification is different from the algorithm applied previously to image reconstruction. Correspondingly, we also reach some new conclusion: the tolerance for fiber bending in image classification is dramatically higher than the tolerance previously found for image reconstruction.

Apart from the great success already shown, further work can be made in several ways to study as well as to enhance the performance of the GALOF-based system. First, features of the objects, such as brightness, cell sizes and clustering, can greatly affect the classification performance. To explore the limitations of the system regarding the classification of objects with increasing similarity, further studies are needed. Secondly, a direct comparison among GALOF-based, MMF-based, and MCF-based systems on object recognition under perturbations lacks in literature. The current discussion is based on their performances on image acquisition. However, since image acquisition is a more demanding task than object recognition, high sensitivity of the transmission matrix to perturbations in image acquisition should not rule out the possibility of MMF-based and MCF-based systems' applications in robust object recognition. It is possible that despite large changes in the output images, some underlying patterns are preserved, which can be utilized to categorize different objects. This is beyond the scope of this work and requires further studies. Thirdly, a smaller localization length is preferable to achieve higher imaging resolution and increased classification accuracy. It has been shown that an air-filling fraction of $\sim$50%, an average air-hole diameter of about twice the operating wavelength and a high refractive index variation can result in small localization lengths [63], [71]–[73]. The current GALOF has an air-filling fraction of $\sim$28.5% and an average air-hole diameter of $\sim$1.6 μm. Thus, future work can be done to optimize the GALOF geometry and perhaps its material composition. Furthermore, a reflection mode operation is more favorable in most practical applications. That is, objects should be recognized from the backscattered light instead of the transmitted light as in the current setup. Therefore, we will investigate next-generation GALOF-based systems that include illuminating light guided either through parts of the disordered structure or through the non-disordered GALOF cladding. Lastly, new ideas to optimize DCNN architectures and training procedures will help to improve the performance of FOISs and open new application areas.

IV. Conclusion

We show that even though the original image of the object is scrambled, abundant information is preserved during light transmission through the GALOF. The demonstrated high accuracy of the trained DCNN in classifying unseen complex objects even when the fiber is strongly bent indicates the robustness of the information transport through GALOF. We see great potentials for our GALOF-based FOIS in endoscopy applications that require high-quality imaging [59], [60] and reliable object classification.

References

[1] B. A. Flusberg, E. D. Cocker, W. Piyawattanametha, J. C. Jung, E. L. M. Cheung, and M. J. Schnitzer, "Fiber-optic fluorescence imaging," *Nat. Methods*, vol. 2, no. 12, pp. 941–950, Dec. 2005.

[2] F. Koenig, "Diagnosing cancer in vivo," *Science*, vol. 292, no. 5520, pp. 1401–1403, May 2001.

[3] F. Helmchen, M. S. Fee, D. W. Tank, and W. Denk, "A miniature head-mounted two-photon microscope," *Neuron*, vol. 31, no. 6, pp. 903–912, Sep. 2001.

[4] V. Szabo, C. Ventalon, V. De Sars, J. Bradley, and V. Emiliani, "Spatially selective holographic photoactivation and functional fluorescence imaging in freely behaving mice with a fiberscope," *Neuron*, vol. 84, no. 6, pp. 1157–1169, Dec. 2014.

[5] Y. Chang, W. Lin, J. Cheng, and S. C. Chen, "Compact high-resolution endomicroscopy based on fiber bundles and image stitching," *Opt. Lett.*, vol. 43, no. 17, Sep. 2018, Art. no. 4168.

[6] T. J. Muldoon, M. C. Pierce, D. L. Nida, M. D. Williams, A. Gillenwater, and R. Richards-Kortum, "Subcellular-resolution molecular imaging within living tissue by fiber microendoscopy," *Opt. Express*, vol. 15, no. 25, Dec. 2007, Art. no. 16413.

[7] M. Hughes, T. P. Chang, and G.-Z. Yang, "Fiber bundle endocytoscopy," *Biomed. Opt. Express*, vol. 4, no. 12, Dec. 2013, Art. no. 2781.

[8] A. Perperidis, K. Dhaliwal, S. McLaughlin, and T. Vercauteren, "Image computing for fibre-bundle endomicroscopy: A review," *Medical Image Analysis*, vol. 62, May 2020, Art. no. 101620.

[9] D. Kim *et al.*, "Toward a miniature endomicroscope: pixelation-free and diffraction-limited imaging through a fiber bundle," *Opt. Lett.*, vol. 39, no. 7, Apr. 2014, Art. no. 1921.

[10] U. Weiss and O. Katz, "Two-photon lensless micro-endoscopy with in-situ wavefront correction," *Opt. Express*, vol. 26, no. 22, Oct. 2018, Art. no. 28808.

[11] V. Tsvirkun, S. Sivankutty, G. Bouwmans, O. Katz, E. R. Andresen, and H. Rigneault, "Widefield lensless endoscopy with a multicore fiber," *Opt. Lett.*, vol. 41, no. 20, Oct. 2016, Art. no. 4771.

[12] E. R. Andresen, S. Sivankutty, V. Tsvirkun, G. Bouwmans, and H. Rigneault, "Ultrathin endoscopes based on multicore fibers and adaptive optics: A status review and perspectives," *J. Biomed. Opt*, vol. 21, no. 12, Oct. 2016, Art. no. 121506.

[13] T. Čižmár and K. Dholakia, "Exploiting multimode waveguides for pure fibre-based imaging," *Nat Commun*, vol. 3, no. 1, Jan. 2012, Art. no. 1027.

[14] Y. Choi *et al.*, "Scanner-free and wide-field endoscopic imaging by using a single multimode optical fiber," *Phys. Rev. Lett.*, vol. 109, no. 20, Nov. 2012, Art. no. 203901.

[15] I. N. Papadopoulos, S. Farahi, C. Moser, and D. Psaltis, "High-resolution, lensless endoscope based on digital scanning through a multimode optical fiber," *Biomed. Opt. Express*, vol. 4, no. 2, pp. 260–270, Feb. 2013.

[16] S. Ohayon, A. Caravaca-Aguirre, R. Piestun, and J. J. DiCarlo, "Minimally invasive multimode optical fiber microendoscope for deep brain fluorescence imaging," *Biomed. Opt. Express*, vol. 9, no. 4, Apr. 2018, Art. no. 1492.

[17] B. Münzer, K. Schoeffmann, and L. Böszörmenyi, "Content-based processing and analysis of endoscopic images and videos: A survey," *Multimed Tools Appl.*, vol. 77, no. 1, pp. 1323–1362, Jan. 2018.

[18] S. M. Popoff, G. Lerosey, R. Carminati, M. Fink, A. C. Boccara, and S. Gigan, "Measuring the transmission matrix in optics: an approach to the study and control of light propagation in disordered media," *Physical Rev. Lett.*, vol. 104, p. 100601, 2010.

[19] T. Čižmár and K. Dholakia, "Shaping the light transmission through a multimode optical fibre: complex transformation analysis and applications in biophotonics," *Opt. Express*, vol. 19, no. 20, Sep. 2011, Art. no. 18871.

[20] S. Turtaev, I. T. Leite, T. Altwegg-Boussac, J. M. P. Pakan, N. L. Rochefort, and T. Čižmár, "High-fidelity multimode fibre-based endoscopy for deep brain in vivo imaging," *Light Sci. Appl.*, vol. 7, no. 1, pp. 1–8, Dec. 2018.

[21] M. Plöschner, T. Tyc, and T. Čižmár, "Seeing through chaos in multimode fibres," *Nature Photon.*, vol. 9, no. 8, pp. 529–535, Aug. 2015.

[22] B. Rahmani, D. Loterie, G. Konstantinou, D. Psaltis, and C. Moser, "Multimode optical fiber transmission with a deep learning network," *Light Sci. Appl.*, vol. 7, no. 1, pp. 1–11, Dec. 2018.

[23] N. Borhani, E. Kakkava, C. Moser, and D. Psaltis, "Learning to see through multimode fibers," *Optica*, vol. 5, no. 8, pp. 960–966, Aug. 2018.

[24] N. Shabairou, E. Cohen, O. Wagner, D. Malka, and Z. Zalevsky, "Color image identification and reconstruction using artificial neural networks on multimode fiber images: towards an all-optical design," *Opt. Lett.*, vol. 43, no. 22, Nov. 2018, Art. no. 5603.

[25] P. Caramazza, O. Moran, R. Murray-Smith, and D. Faccio, "Transmission of natural scene images through a multimode fibre," *Nat Commun*, vol. 10, no. 1, Dec. 2019, Art. no. 2029.

[26] Y. LeCun, Y. Bengio, and G. Hinton, "Deep learning," *Nature*, vol. 521, no. 7553, pp. 436–444, May 2015.

[27] D. Shen, G. Wu, and H.-I. Suk, "Deep learning in medical image analysis," *Ann. Rev. Biomed. Eng.*, vol. 19, pp. 221–248, 2017.

[28] G. Litjens *et al.*, "A survey on deep learning in medical image analysis," *Med. Image Anal.*, vol. 42, pp. 60–88, Dec. 2017.

[29] D. Ravi *et al.*, "Deep Learning for Health Informatics," *IEEE J. Biomed. Health Inform.*, vol. 21, no. 1, pp. 4–21, Jan. 2017.

[30] E. Valent and Y. Silberberg, "Scatterer recognition via analysis of speckle patterns," *Optica*, vol. 5, no. 2, pp. 204–207, Feb. 2018.

[31] G. Kim, S. Kapetanovic, R. Palmer, and R. Menon, "Lensless-camera based machine learning for image classification," 2017, *arXiv:1709.00408*.

[32] T. Ando, R. Horisaki, and J. Tanida, "Speckle-learning-based object recognition through scattering media," *Opt. Express*, vol. 23, no. 26, Dec. 2015, Art. no. 33902.

[33] G. Satat, M. Tancik, O. Gupta, B. Heshmat, and R. Raskar, "Object classification through scattering media with deep learning on time resolved measurement," *Opt. Express*, vol. 25, no. 15, Jul. 2017, Art. no. 17466.

[34] Y. Tan, X. Lei, K. X. Wang, S. Fan, and Z. Yu, "Imaging-free object recognition enabled by optical coherence," 2019, *arXiv:1901.08118*.

[35] S. Aisawa, K. Noguchi, and T. Matsumoto, "Remote image classification through multimode optical fiber using a neural network," *Opt. Lett.*, vol. 16, no. 9, pp. 645–647, May 1991.

[36] T. Matsumoto, M. Koga, K. Noguchi, and S. Aizawa, "Proposal for neural-network applications to fiber-optic transmission," in *Proc. 1990 IJCNN Int. Joint Conf. Neural Netw.*, San Diego, CA, USA, 1990, vol. 1, pp. 75–80.

[37] R. K. Marusarz and M. R. Sayeh, "Neural network-based multimode fiber-optic information transmission," *Appl. Opt.*, vol. 40, no. 2, pp. 219–227, Jan. 2001.

[38] R. Takagi, R. Horisaki, and J. Tanida, "Object recognition through a multimode fiber," *Opt. Rev.*, vol. 24, no. 2, pp. 117–120, Apr. 2017.

[39] P. Wang and J. Di, "Deep learning-based object classification through multimode fiber via a CNN-architecture SpeckleNet," *Appl. Opt.*, vol. 57, no. 28, Oct. 2018, Art. no. 8258.

[40] E. Kakkava, N. Borhani, B. Rahmani, U. Teğin, C. Moser, and D. Psaltis, "Deep learning-based image classification through a multimode fiber in the presence of wavelength drift," *Appl. Sci.*, vol. 10, no. 11, May 2020, Art. no. 3816.

[41] J. A. Grant-Jacob *et al.*, "Fibre-optic based particle sensing via deep learning," *J. Phys.: Photon.*, vol. 1, no. 4, Sep. 2019, Art. no. 044004.

[42] K. L. Reichenbach and C. Xu, "Numerical analysis of light propagation in image fibers or coherent fiber bundles," *Opt. Express*, vol. 15, no. 5, 2007, Art. no. 2151.

[43] X. Chen, K. L. Reichenbach, and C. Xu, "Experimental and theoretical analysis of core-to-core coupling on fiber bundle imaging," *Opt. Express*, vol. 16, no. 26, Dec. 2008, Art. no. 21598.

[44] A. M. Caravaca-Aguirre and R. Piestun, "Single multimode fiber endoscope," *Opt. Express*, vol. 25, no. 3, Feb. 2017, Art. no. 1656.

[45] A. M. Caravaca-Aguirre, E. Niv, D. B. Conkey, and R. Piestun, "Real-time resilient focusing through a bending multimode fiber," *Opt. Express*, vol. 21, no. 10, May 2013, Art. no. 12881.

[46] R. Kuschmierz, E. Scharf, N. Koukourakis, and J. W. Czarske, "Self-calibration of lensless holographic endoscope using programmable guide stars," *Opt. Lett.*, vol. 43, no. 12, Jun. 2018, Art. no. 2997.

[47] D. Loterie, D. Psaltis, and C. Moser, "Bend translation in multimode fiber imaging," *Opt. Express*, vol. 25, no. 6, Mar. 2017, Art. no. 6263.

[48] S. Farahi, D. Ziegler, I. N. Papadopoulos, D. Psaltis, and C. Moser, "Dynamic bending compensation while focusing through a multimode fiber," *Opt. Express*, vol. 21, no. 19, Sep. 2013, Art. no. 22504.

[49] M. Lan, D. Guan, L. Gao, J. Li, S. Yu, and G. Wu, "Robust compressive multimode fiber imaging against bending with enhanced depth of field," *Opt. Express*, vol. 27, no. 9, Apr. 2019, Art. no. 12957.

[50] D. E. Boonzajer Flaes, J. Stopka, S. Turtaev, J. F. de Boer, T. Tyc, and T. Čižmár, "Robustness of light-transport processes to bending deformations in graded-index multimode waveguides," *Phys. Rev. Lett.*, vol. 120, no. 23, Jun. 2018, Art. no. 233901.

[51] P. Fan, T. Zhao, and L. Su, "Deep learning the high variability and randomness inside multimode fibres," Jul. 2018, Accessed: Jun. 12, 2020, [Online]. Available: http://arxiv.org/abs/1807.09351

[52] T. Schwartz, G. Bartal, S. Fishman, and M. Segev, "Transport and Anderson localization in disordered 2-D photonic lattices," *Nature*, vol. 446, no. 7131, pp. 52–55, Mar. 2007.

[53] S. Karbasi, C. R. Mirr, P. G. Yarandi, R. J. Frazier, K. W. Koch, and A. Mafi, "Observation of transverse Anderson localization in an optical fiber," *Opt. Lett.*, vol. 37, no. 12, Jun. 2012, Art. no. 2304.

[54] S. Karbasi, R. J. Frazier, K. W. Koch, T. Hawkins, J. Ballato, and A. Mafi, "Image transport through a disordered optical fibre mediated by transverse Anderson localization," *Nat Commun*, vol. 5, no. 1, May 2014, Art. no. 3362.

[55] A. Mafi, "Transverse Anderson localization of light: A tutorial," *Adv. Opt. Photon.*, vol. 7, no. 3, pp. 459–515, Sep. 2015.

[56] S. Karbasi, T. Hawkins, J. Ballato, K. W. Koch, and A. Mafi, "Transverse Anderson localization in a disordered glass optical fiber," *Opt. Mater. Express*, vol. 2, no. 11, Nov. 2012, Art. no. 1496.

[57] M. Chen and M.-J. Li, "Observing transverse Anderson localization in random air line based fiber," 2014, pp. 89941S–89941.
[58] J. Zhao *et al.*, "Image transport through meter-long randomly disordered silica-air optical fiber," *Sci Rep*, vol. 8, no. 1, Dec. 2018, Art. no. 3065.
[59] J. Zhao *et al.*, "Deep learning imaging through fully-flexible glass-air disordered fiber," *ACS Photon.*, vol. 5, no. 10, pp. 3930–3935, Oct. 2018.
[60] J. Zhao *et al.*, "Deep-learning cell imaging through Anderson localizing optical fiber," *Adv. Photon.*, vol. 1, no. 6, pp. 1–12, Nov. 2019.
[61] A. Mafi, J. Ballato, K. W. Koch, and A. Schulzgen, "Disordered anderson localization optical fibers for image transport—A review," *J. Lightw. Technol.*, vol. 37, no. 22, pp. 5652–5659, Nov. 2019.
[62] B. Abaie *et al.*, "Disorder-induced high-quality wavefront in an Anderson localizing optical fiber," *Optica*, vol. 5, no. 8, pp. 984–987, Aug. 2018.
[63] S. Karbasi, C. R. Mirr, R. J. Frazier, P. G. Yarandi, K. W. Koch, and A. Mafi, "Detailed investigation of the impact of the fiber design parameters on the transverse Anderson localization of light in disordered optical fibers," *Opt. Express*, vol. 20, no. 17, Aug. 2012, Art. no. 18692.
[64] G. Ruocco, B. Abaie, W. Schirmacher, A. Mafi, and M. Leonetti, "Disorder-induced single-mode transmission," *Nat. Commun*, vol. 8, no. 1, Apr. 2017, Art. no. 14571.
[65] W. Schirmacher, B. Abaie, A. Mafi, G. Ruocco, and M. Leonetti, "What is the right theory for Anderson localization of light? An experimental test," *Phys. Rev. Lett.*, vol. 120, no. 6, Feb. 2018, Art. no. 067401.
[66] K. Simonyan and A. Zisserman, "Very deep convolutional networks for large-scale image recognition," Accessed: Jun. 16, 2020, [Online]. Available: http://arxiv.org/abs/1409.1556
[67] X. Glorot and Y. Bengio, "Understanding the difficulty of training deep feedforward neural networks," in *Proc. 13th Int. Conf. Artif. Intell. Statist., Proc. Machine Learn. Research*, 2010.
[68] D. P. Kingma and J. Ba, "Adam: A method for stochastic optimization,", Accessed: Jun. 16, 2020, [Online]. Available: http://arxiv.org/abs/1412.6980
[69] N. Srivastava, G. Hinton, A. Krizhevsky, I. Sutskever, and R. Salakhutdinov, "Dropout: A simple way to prevent neural networks from Overfitting," *J. Mach. Learn. Res.*, vol. 15, pp. 1929–1958, 2014.
[70] S. Karbasi, K. W. Koch, and A. Mafi, "Multiple-beam propagation in an Anderson localized optical fiber," *Opt. Express*, vol. 21, no. 1, pp. 305–313, Jan. 2013.
[71] S. Karbasi, K. W. Koch, and A. Mafi, "Modal perspective on the transverse Anderson localization of light in disordered optical lattices," *J. Opt. Soc. Amer. B*, vol. 30, no. 6, Jun. 2013, Art. no. 1452.
[72] S. Karbasi, K. W. Koch, and A. Mafi, "Image transport quality can be improved in disordered waveguides," *Opt. Commun.*, vol. 311, pp. 72–76, Jan. 2013.
[73] H. De Raedt, A. Lagendijk, and P. de Vries, "Transverse localization of light," *Phys. Rev. Lett.*, vol. 62, no. 1, pp. 47–50, Jan. 1989.

Xiaowen Hu received the B.S. degree in optical science and technology from Fudan University, China, in 2015. He is currently working toward the Ph.D. degree in optics and photonics with CREOL, The College of Optics and Photonics, University of Central Florida, FL, USA. His research interests include microstructured fiber optics, machine learning applications in optics, and optical fiber imaging.

Jian Zhao received the B.S. and Ph.D. degrees in optics from the School of Physics and Engineering, Sun Yat-sen University, China, and from CREOL, University of Central Florida, United States, respectively. He is a Postdoctoral Associate with the Department of Electrical & Computer Engineering, Boston University, Boston, Massachusetts, United States. His research interests include bio-imaging, deep learning in optics, fiber optics, and ultrafast optics. He is a member of SPIE and OSA.

Jose E. Antonio-Lopez, biography is not available at the time of publication.

Shengli Fan received the B.S. degree in optical science and technology from the School of Science, Harbin Institute of Technology, Shandong, China, in 2014. He is currently working toward the Ph.D. degree in optics with the College of Optics and Photonics, University of Central Florida, Orlando, FL, USA. His research interests include optical imaging, microscopy, inverse problem, and signal processing.

Rodrigo Amezcua Correa, biography is not available at the time of publication.

Axel Schülzgen (Fellow) received the Ph.D. degree in physics from the Humboldt-University of Berlin, Germany. Since 2009, he has been a Professor of Optics and Photonics with CREOL, The College of Optics and Photonics, University of Central Florida, FL, USA. He also holds an Adjunct Research Professor position with the College of Optical Sciences, University of Arizona. He authored more than 130 scientific publications in peer reviewed journals, over 60 invited talks at international conferences, and 6 patents. His current research interests include optical fiber devices, components, materials, and structures with applications in fiber laser systems, fiber optic sensing and imaging, and optical communications. Dr. Schülzgen is a Fellow of the Optical Society of America.